Optics Letters

Real-time fully digital control scheme for pulse coherent beam combining

Yong Wu,[1] Xinyu Wang,[2] Guoqing Pu,[1,3] Xuguang Zhang,[1] Chenxu Liu,[2] Kegong Dong,[2] Weisheng Hu,[1] and Lilin Yi[1,*]

[1]State Key Lab of Advanced Communication Systems and Networks, School of Electronic Information and Electrical Engineering, Shanghai Jiao Tong University, Shanghai 200240, China
[2]Laser Fusion Research Center, Chinese Academy of Engineering Physics, Mianyang 621900, China
[3]teddyghf1994@sjtu.edu.cn
*lilinyi@sjtu.edu.cn

Received 21 August 2024; revised 22 September 2024; accepted 8 October 2024; posted 9 October 2024; published 1 November 2024

A fully digital control scheme for non-polarization-maintaining (non-PM) nanosecond pulse coherent beam combining (CBC) is proposed, where digital locking of optical coherence by single-detector electronic-frequency tagging (LOCSET) for active phase control and stochastic parallel gradient descent (SPGD) for active polarization control is proposed. The fully digital control scheme is integrated on a real-time field-programmable gate array (FPGA) empowered hardware platform and then experimentally validated in a four-channel all-fiber non-fully polarization-maintaining nanosecond pulse CBC system. Consequently, the system can be fully locked in 9.5 ms, and the polarization extinction ratio (PER) of the combined beam is 21.5 dB with a CBC efficiency of 95.3%. The fully digital control scheme integrates the advantages of digital LOCSET and multi-channel active polarization control, enhancing the channel scalability and the potential output power of the non-PM pulse CBC system.

https://doi.org/10.1364/OL.539854

High-power nanosecond pulsed fiber lasers with linear polarization and decent beam quality have extensive applications in various fields such as laser processing [1], nonlinear frequency conversion [2], laser lidar [3], and terahertz technology [4]. Due to the inherent nonlinearity inside the fiber [5], which is exacerbated in pulsed systems, the power output from a single fiber channel is limited. Consequently, coherent beam combining (CBC) of multiple channels has emerged as an extremely effective strategy for power scaling, owing to its high efficiency and good beam quality. Pulse CBC needs all beams in multiple channels to be coherent, which means they should be temporally synchronized, frequency matched, phase matched, and co-polarized.

Serval control schemes are proposed to achieve active phase control for pulse CBC, including the Hänsch–Couillaud detection [6], optical heterodyne detection [7], stochastic parallel gradient descent (SPGD) [8], and locking of optical coherence by single-detector electronic-frequency tagging (LOCSET) [9,10]. The latter two techniques require only a single detector. Notably, compared to SPGD, the bandwidth of LOCSET would not decrease with the increase in the number of channels. The disadvantage of LOCSET originates from the complex analog local oscillator and coherent demodulation circuits demanding complicated synchronization. Digital modulation and demodulation will offer an effective and elegant solution to address the issues.

Compared to polarization-maintaining (PM) systems, non-polarization-maintaining (non-PM) systems offer higher power of a single-mode output due to the difference in the waveguide asymmetry [11,12]. Additionally, previous studies indicate that PM fiber amplifiers have notably lower TMI thresholds than non-PM versions [13,14]. As a result, active polarization control is also crucial in kilowatt-level non-PM fiber amplifier systems. However, active polarization control is not considered in pulse CBC. In the tiled-aperture pulse CBC setup, the polarization alignment is resolved by the utilization of the all-polarization-maintaining system [15]. Alternatively, manual polarization tuning is required to align the SOP of multiple channels in the spatial polarization beam combining of the filled-aperture pulse CBC setup [16,17]. Particularly, both tiled-aperture and filled-aperture pulse CBC schemes incorporate PM fiber components. Compared to non-PM systems, the combined power of current pulse CBC is limited. Hence, non-PM pulse CBC with active polarization control to break the power limit is imperative and remains unexplored.

In this Letter, we propose a fully digital control scheme containing both active phase and polarization control for the pulse CBC system. We employ the all-digital signal processing LOCSET for active phase control in the pulse CBC system. Furthermore, we employ the SPGD algorithm for active polarization control to achieve the desired linear polarization for each channel, potentially offering higher power compared to PM systems due to the difference in the waveguide asymmetry. The proposed scheme is integrated on a real-time FPGA-empowered hardware platform and then experimentally validated in a four-channel all-fiber nanosecond pulse CBC system, which can be

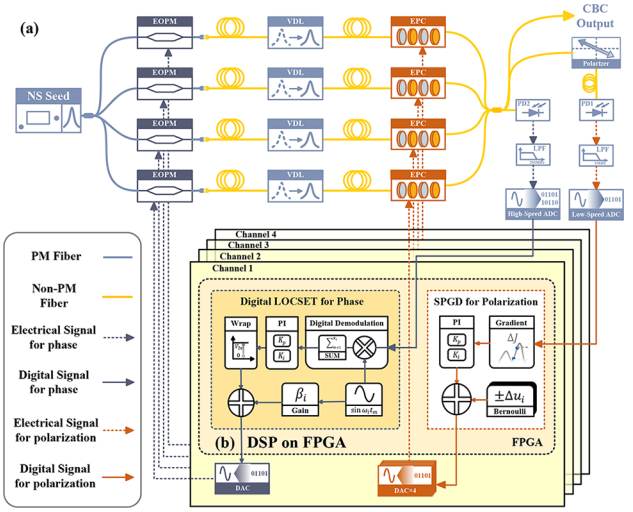

Fig. 1. (a) Experimental setup of a four-channel nanosecond pulse CBC system incorporating active phase and polarization control. (b) Digital signal processing (DSP) flow chart of active phase control (left, digital LOCSET) and active polarization control (right, SPGD).

fully locked within 9.5 ms with the PER of 21.5 dB and the CBC efficiency of 95.3%.

The electrical polarization controller (EPC) controls the state of polarization (SOP) through an orderly arrangement of four retarders inside the controller, set at azimuths of 0°, 45°, −45°, and 0°, respectively. One retarder can be expressed with the Jones matrix as Eq. (1):

$$\vec{\mathbf{J}} = \begin{bmatrix} \cos\theta & -\sin\theta \\ \sin\theta & \cos\theta \end{bmatrix} \begin{bmatrix} e^{i\delta/2} & 0 \\ 0 & e^{-i\delta/2} \end{bmatrix} \begin{bmatrix} \cos\theta & \sin\theta \\ -\sin\theta & \cos\theta \end{bmatrix}, \quad (1)$$

where θ is the fixed azimuths and δ is the phase retardance of the retarder [18]. Obviously, altering the SOP of the beam through an EPC will inherently affect the phase of the beam, impacting both the x and y components. Therefore, directly combining polarization and phase control can result in mutual cross talk with each other. Naturally, if δ undergoes only minor changes, the overall phase change will also be minimal. Given the fact that the phase noise typically occur at the kHz level [19] and polarization generally varies slowly on the order of hours to days for installed fibers [20], we use a strategy that prioritizes phase locking to the polarization optimization. Otherwise, the feedback signal variation during polarization control may also raise from phase perturbations, leading to misjudgments in polarization control. The separate locking strategy effectively avoids the overlap of EPC and phase modulator control, thereby accelerating the convergence. Moreover, even though the bandwidth of SPGD decreases with an increasing number of channels, the inherently modest bandwidth requirements of polarization control allow the scheme to retain the advantage of channel scalability offered by LOCSET.

To validate the proposed scheme, we establish a four-channel nanosecond pulse all-fiber coherent beam combing system with active phase and polarization control as shown in Fig. 1(a). The seed is a 1064-nm nanosecond pulse source with a duration of ∼10 ns and a repetition rate of 1 MHz. Then it is split into four fiber channels, each containing a $LiNO_3$ electro-optic phase modulator (EOPM) with a half-wave voltage of 2.4 V and a 300-MHz operating bandwidth. The PM fiber used here is just due to the polarization-maintaining property of the EOPM. The response time of the EOPM is also the critical parameter to phase control and is further discussed later. We utilize non-PM variable delay lines (VDLs) with a precision of 0.01 ps to adjust the optical path length matched across multiple channels. The precise delay calibration is completed by replacing the nanosecond pulse source with a picosecond pulse source and then temporally superposing picosecond pulses coming out from different channels detected by a high-speed real-time oscilloscope. Each channel is also equipped with a commercial EPC. The SOP is controlled through an orderly arrangement of four retarders inside the EPC, set at azimuths of 0°, 45°, −45°, and 0°, respectively. Subsequently, the four optical paths are coupled together through a fiber coupler for coherent beam combining, which also work for other CBC geometries such as tiled-aperture and filled-aperture geometries. The non-PM fiber amplifiers can also be utilized after EPCs to obtain linear-polarization higher-power combined beam in pulse CBC. Two taps from the output beam are used for detection, which are separately responsible for active phase and polarization control. The feedback path for active phase control is sampled by a high-speed ADC (370 MSPS, AD9434) after photodetector and low-pass filtering (LPF) with a 3-dB bandwidth of 200 MHz. The alternative path serving for active polarization control first passes through a polarizer, then undergoes low-pass filtering with a 3-dB bandwidth of 10 kHz, and finally being sampled by a low-speed ADC (20 MSPS, LTC2201). As for the output section, the control of the EOPM employed a 12-bit high-speed DAC (20.4 MSPS, DAC7821) spanning a 0–5-V range of the output voltage. A single EPC required four DACs (2.7 MSPS, AD5444), with the output voltage controlled in 0 V–4 V. Through the driver of the EPC, the output voltage of DACs can be amplified to a maximum of 350 V DC to ensure the phase of each retarder exceeding a range of 2π rad, thereby enabling the SOP to traverse the entire Poincaré sphere.

The fully digital control scheme is depicted in Fig. 1(b) involving the transformation of feedback electrical signals through a series of algorithmic steps, implemented on a Xilinx Zynq 7000 series FPGA. The digital LOCSET, highlighted in a darker yellow box on the left in Fig. 1(b), aims to circumvent the use of a fixed circuit oscillator, a key component to synchronize multiple channels in the conventional LOCSET. This approach substantially enhances the scalability and flexibility of the system, as the fully digital domain processing allows for easier adjustments and optimizations. Each channel is independently processed the signal in parallel. Initially, for each channel, a digital sine generator module produces a sinusoidal dither signal with the amplitude of $\lambda/76$ loaded on the EOPM. In the digital demodulation module, the feedback signal multiplies the identical sinusoidal dither signal with tunable delay and then is integrated the product to obtain the overall phase difference on the current channel in the digital domain. Subsequently, the demodulated phase difference is transformed to the control voltage through a proportional–integral (PI) controller. Finally, a phase wrapper algorithm is employed to prevent the voltage from exceeding the limit. Specifically, it is adjusted by adding or subtracting $2V_\pi$ to ensure the voltage stays within $[0, 2V_\pi + \Delta V]$ since the output voltages of the high-speed DACs are all positive. Furthermore, to avoid rapid flipping of the phase control signal between 0 and $2V_\pi$, there is ΔV tolerance in the voltage [21], and the sinusoidal dither signal employed is added with a bias equal to its amplitude.

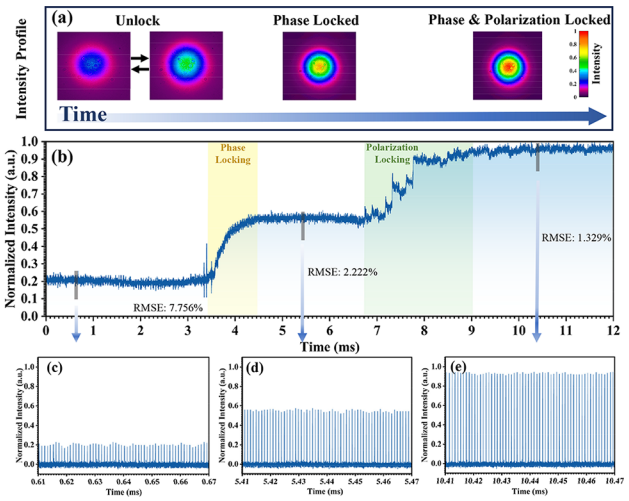

Fig. 2. (a) Intensity profiles of the combined beam through a polarizer measured by CCD during the whole process from open loop to closed loop. (b) Normalized peak intensity of the combined pulse train through a polarizer recorded by an oscilloscope. The corresponding RMSE of the peak intensity in three white regions is calculated. (c)–(e) Combined pulse signals correspond to the gray areas in (b).

SPGD is employed on the processing system (PS) of the FPGA to realize active polarization control, as shown in the white box in Fig. 1(b). The perturbation signal, denoted as Δu_i, follows a Bernoulli distribution [22] with a fixed amplitude. The dither used in experiments is 0.02 V to solve the gradient from the signal after low-pass filtering. Likewise, a PI controller is utilized to map the computed gradient to the control voltage of the EPC. Each EPC needs four voltage signals, and a total of 16 DACs are employed to control the polarization of the CBC system. Since three retarders can traverse the entire Poincaré sphere, we utilize the remaining retarder as a corrective measure for endless recovery [23] in polarization control, thereby avoiding a jump between 0 and $2V_\pi$ at the boundaries. Figure 2(a) illustrates the evolution of the combined beam intensity profile recorded by a CCD (Spiricon, SP620U) during the entire active control. This process can be divided into three stages. The first stage is the unlocked stage. Due to the high sensitivity of the optical phase to external environmental vibrations and temperature drifts, the intensity of the beam is relatively low and fluctuates in brightness without phase control. Conversely, the combined beam comes stable and strong immediately with phase locked. Active polarization locking is performed after phase locked, resulting in a stable linearly polarized beam with greater intensity.

Figure 2(b) illustrates the intensity of the output beam after passing through a polarizer during the whole locking process. The original signal after the photodetector (PD), a series of pulses, is recorded by an oscilloscope at a sampling rate of 100 MSPS. For better visualization, we extract the peak of each pulse and plot the curve in Fig. 2(b). The three white regions correspond to the intensity profile in Fig. 2(a), which represent the three stages of the whole process, and their RMS intensity stabilities are respectively 7.756%, 2.222%, and 1.329%. The yellow region represents the phase locking process enabled by digital LOCSET, with the convergence time of approximately 0.7 ms. When the phase is not locked, significant intensity fluctuations are observed in the feedback signal for active polarization control. Consequently, accurate gradient is unavailable

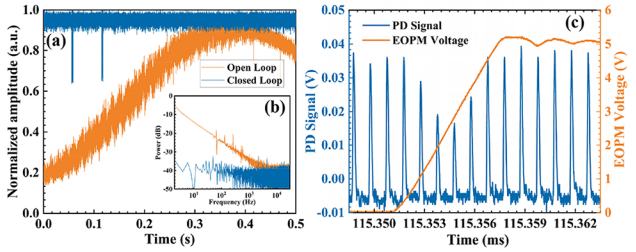

Fig. 3. (a) Normalized energy of the combined pulse train when phase control is on (blue line) and off (orange line), and the corresponding FFT spectra shown in (b). (c) Sudden drop of pulse energy in (a); the blue line shows the raw pulse signal of photodetector (PD), and the orange line represents the voltage of the EOPM.

to align polarization when the phase is unlocked. Therefore, it is necessary to lock the phase before active polarization control. The green region indicates the polarization control process with the SPGD and the convergence time ranges in 1 ms–8 ms, depending on the initial SOPs of the four channels. A distinct stair-step pattern can be observed in the polarization control process, which is attributed to the ~50 μs response time of the EPC. Therefore, the time consumption of active polarization control can be further reduced by using a faster EPC. Note that the white region between the phase locking and polarization locking in Fig. 2(b) is deliberately delayed to distinguish the convergence of the phase locking and polarization locking. In the actual system, the overall convergence can be achieved within 1 ms–9.5 ms, which is substantially subject to the polarization locking. Figures 2(c)–2(e) show pulses corresponding to the gray regions in Fig. 2(b). Due to the different channel losses of the systems, prior to coherent beam combining, the average powers of the four channels at the output of the combiner are respectively 0.5957 mW, 0.5058 mW, 0.5715 mW, and 0.3681 mW. The average power after CBC is 1.9454 mW and the combining efficiency of 95.31% is achieved. To characterize the phase control performance of the system, we record the original pulse under phase-locked and phase-unlocked states for a period. Limited by the record length of the oscilloscope at a sampling rate of 100 MSPS, the data length is 0.5 s and there are ~30 points sampled per pulse. Normalized pulse energy [10] is extracted from the collected data, as shown in Fig. 3(a). The mean normalized pulse energy under the phase-locked state is 0.9517, with the RMSE of 1.2419%. The corresponding residual phase error is 0.2229 rad, which is ~ $\lambda/27$, according to Eq. (2):

$$\Delta\phi_{rms} = 2\sqrt{\frac{\Delta V_{rms}}{V_{max}}}, \tag{2}$$

where $V(t)$ is the energy evolution of the pulses [10]. The residual phase error also matches the efficiency according to the expression $\Delta\phi_{rms} = \sqrt{1-\eta}$ [24]. Moreover, a spectral analysis is also performed on the collected data using FFT as shown in the inset of Fig. 3(b). It is obvious that the noise components below 5 kHz are well suppressed, which can be approximately considered as the effective control bandwidth of the phase control. This is consistent with the actual system parameters, where the tagging frequencies are 120 kHz, 135.7 kHz, and 154 kHz.

There are sudden drops of approximately 40% in the pulse energy when the phase is locked in Fig. 3(a), which originate from the phase wrapper algorithm. Due to the response time of the EOPM, when the phase exceeds the boundary value of 0 or

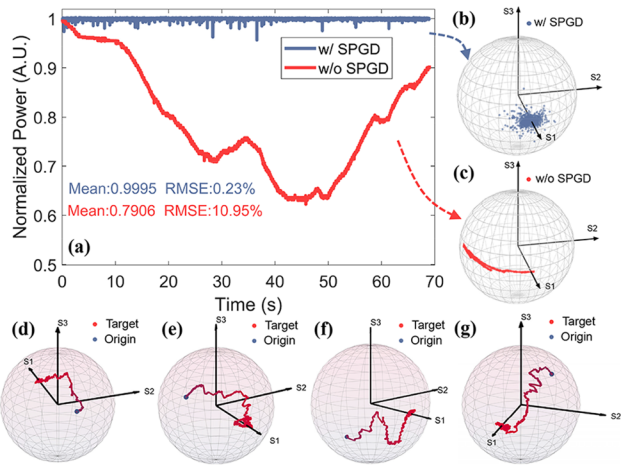

Fig. 4. (a) Power of the combined beam through a polarizer over 70 s with (blue) and without (red) active polarization control and the corresponding SOP traces shown in (b) and (c). (d)–(g) show SOP traces during polarization locking with different initial SOP.

$2V_\pi$, the actual voltage of the EOPM does not directly jump to the target voltage but changes monotonously like the yellow line in Fig. 3(c). This causes the actual optical path phase difference to first increase to π and then decrease to zero, thus resulting in the pulse intensity drop. On the other hand, the sudden drop in the pulse intensity is equivalent to apply an additional phase difference to the channels, resulting in a significant deviation in the integral result. More detrimentally, this deviation continues to affect the demodulation of the next period, potentially causing pulses to oscillate cyclically. To address this challenge, we implement an automatic pause mechanism in the demodulation of the digital LOCSET. When the phase jumping between 0 and $2V_\pi$ is detected, the algorithm automatically pauses for a period of time to prevent the calculation over erroneous pulses. Because the dither of each channel is digital as shown in Fig. 1(b), the automatic pause mechanism can be easily implemented in the digital LOCSET. Figure 4(a) shows the power of the combined beam through a polarizer over 70 s with and without active polarization control under the phase-locked state. Figure 4(c) depicts the corresponding evolution of the SOP, which is recorded using a polarimeter (Thorlabs, PAX1000IR2). Without active polarization control, the SOP of the combined beam slowly drifts away from the target SOP, underscoring the necessity for active polarization control. The demonstrated polarization drift results in a power drop of approximately 40%. This could potentially be attributed to the temperature variations inside the EPCs caused by the high voltages applied to the phase retarders. On the other hand, in non-PM high-power fiber systems, the influence of temperature on the SOP will be greater and more unpredictable due to the high-power amplifiers. Figure 4(b) shows that when active polarization control is on, the SOP remains close to the target linear SOP, and the RMSE of the polarized power in Fig. 4(a) is reduced from 10.95% (blue line) to 0.23% (red line). Figures 4(d)–4(g) represent the situation where four different initial SOPs are guided to the identical linear SOP, verifying the robustness of the polarization control. A portion of the output beam is split by a polarization beam splitter (PBS). The powers on the two branches of the PBS are respectively 0.5636 mW and 0.0045 mW, achieving the PER of 21.5 dB.

In summary, we experimentally demonstrate a real-time fully digital control scheme in a four-channel all-fiber non-fully polarization-maintaining nanosecond pulse CBC system, where the residual phase error of $\sim \lambda/27$, the combining efficiency of 95.3%, and the PER of 21.5 dB are achieved. The digital LOCSET eliminates the complex coherent demodulation circuit in the traditional LOCSET. As a result, the CBC system is cost-effective and easy to support more channels. The overall system is fully locked within 9.5 ms and the locking speed can be further boosted with faster EPCs. By employing EPCs and modulators at different wavelengths, this scheme accommodates arbitrary operating wavelengths used in the CBC domain. It is also compatible with different CBC geometries such as tiled and filled-aperture geometries. The introduction of active polarization control allows the utilization of non-PM fiber amplifiers for higher-power combined beams in pulse CBC. The demonstrated implementation could facilitate the emergence of ultrahigh power pulse source built on CBC.

Funding. National Natural Science Foundation of China (62025503, 62205199, 62227821).

Disclosures. The authors declare no conflicts of interest.

Data availability. Data underlying the results presented in this paper are not publicly available at this time but may be obtained from the authors upon reasonable request.

REFERENCES

1. X. Jia, J. Dong, Y. Chen, *et al.*, Opt. Lett. **45**, 1691 (2020).
2. D. Clarke, J. Phillips, M. Divoky, *et al.*, Opt. Lett. **48**, 6320 (2023).
3. O. Lux, D. Wernham, P. Bravetti, *et al.*, Opt. Lett. **45**, 1443 (2020).
4. Y. Takida, K. Nawata, T. Notake, *et al.*, Opt. Express **30**, 11217 (2022).
5. C. Li, Y. Tao, M. Jiang, *et al.*, Chin. Opt. Lett. **21**, 090002 (2023).
6. A. Klenke, S. Breitkopf, M. Kienel, *et al.*, Opt. Lett. **38**, 2283 (2013).
7. S. Palese, E. Cheung, G. Goodno, *et al.*, Opt. Express **20**, 7422 (2012).
8. R. Su, P. Zhou, X. Wang, *et al.*, Opt. Lett. **37**, 3978 (2012).
9. T. M. Shay, V. Benham, J. T. Baker, *et al.*, Opt. Express **14**, 12015 (2006).
10. V. Jolivet, P. Bourdon, B. Bennai, *et al.*, IEEE J. Sel. Top Quantum Electron. **15**, 257 (2009).
11. G. D. Goodno, S. J. McNaught, J. E. Rothenberg, *et al.*, Opt. Lett. **35**, 1542 (2010).
12. T. Wang, S. Ren, H. Chang, *et al.*, Chin. Opt. Lett. **22**, 041403 (2024).
13. R. Tao, X. Wang, and P. Zhou, IEEE J. Sel. Top Quantum Electron. **24**, 0903319 (2018).
14. G. Palma-Vega, D. Hässner, S. Kuhn, *et al.*, Opt. Express **31**, 24730 (2023).
15. J. L. Dortz, A. Heilmann, M. Antier, *et al.*, Opt. Lett. **42**, 1887 (2017).
16. K. Tsubakimoto, H. Higuchi, K. Fukuishi, *et al.*, Opt. Lett. **44**, 5434 (2019).
17. M. Müller, C. Aleshire, A. Klenke, *et al.*, Opt. Lett. **45**, 3083 (2020).
18. X. J. Chen and X. S. Yao, *Polarization Measurement and Control in Optical Fiber Communication and Sensor Systems* (Wiley, 2023), p. 63.
19. M. Tröbs, P. Wessels, and C. Fallnich, Opt. Lett. **30**, 789 (2005).
20. M. Karlsson, J. Brentel, and P. A. Andrekson, J. Lightwave Technol. **18**, 941 (2000).
21. C. Freier, S. Legge, L. Roberts, *et al.*, Appl. Opt. **61**, 4543 (2022).
22. P. Zhou, Z. Liu, X. Wang, *et al.*, Acta Opt. Sin. **29**, 2232 (2009).
23. R. Noe, H. Heidrich, and D. Hoffmann, J. Lightwave Technol. **6**, 1199 (1988).
24. G. D. Goodno, C.-C. Shih, and J. E. Rothenberg, Opt. Express **18**, 25403 (2010).